ON IF-TO-BASEBAND TRANSLATION AND RESAMPLING IN SAMPLED-DATA RECEIVERS

Michael Rice, Chris Hogstrom, Chris Nash
Department of Electrical & Computer Engineering
Brigham Young University
Provo, Utah, USA
mdr@byu.edu, chris.hogstrom@gmail.com, christopherlarrynash@gmail.com

ABSTRACT

This paper summarizes the design of a discrete-time quadrature downconversion and resampling processor that operates on samples of a 70 MHz IF signal. The unique properties of discrete-time processing—aliasing due to resampling bandpass signals and polyphase filter decompositions—are applied to create a low-complexity approach that does not require any arithmetic operations at the IF sample rate. The required tasks are performed in two stages: a downsample-by-2 operation followed by a more traditional resampler based on a polyphase filterbank.

INTRODUCTION

A fundamental operation in receiver/demodulator front ends is frequency translation from the transmitted radio frequency (RF) to I/Q baseband. This is usually accomplished in two (or more) steps. The first step(s) involve translation from RF to an intermediate frequency (IF). Most receivers used in aeronautical telemetry use the industry-standard 70 MHz as the IF frequency. The last step involves a quadrature mixer and a pair of lowpass filters to produce the inphase component (I) and the quadrature component (Q) in parallel. For digital communications, synchronization, detection filtering, and bit decisions are all performed at I/Q baseband.

The architecture used to accomplish this has evolved as digital technology has matured. The evolution is illustrated in Figure 1. First generation demodulators perform all operations using continuous-time processing as illustrated in Figure 1 (a). The carrier phase PLL is usually closed at the quadrature mixers as shown so as to perform coherent quadrature downconversion. Second-generation demodulators, shown in Figure 1 (b), sample the inphase and quadrature components and perform all the synchronization and detection tasks using discrete-time processing. For this reason, the I/Q downconversion is performed using a free-running VCO tuned to the IF frequency. Third-generation demodulators move the A/D converter to the IF signal and sample the IF signal directly as illustrated in Figure 1 (c). The normal situation is to use bandpass sampling techniques such as those described in [1, Section 2.7].

In third-generation demodulators, the first task performed after sampling is the quadrature downconversion as shown Figure 1 (c). The structure shown here mimics the first-generation continuous-time counterpart. This task can be replaced by more efficient multi-rate processing techniques. The application of multirate discrete-time processing to perform this task is the subject of this paper.

Before proceeding, two items must be kept in mind.

1. The first follows from Euler's formula

$$e^{-j\Omega_0 n} = \cos(\Omega_0 n) - j\sin(\Omega_0 n). \tag{1}$$

   Euler's formula allows for a more compact representation of the quadrature downconversion operation as illustrated in Figure 2. In the figure, single lines indicate real-valued signals whereas double lines indicate complex-valued signals.

2. The second item is the requirement for *resampling*. This is because synchronization and detection require a sample rate equivalent to an integer multiple (usually 2 or 4) of the bit rate. Because it is rare that the IF sample rate $(1/T)$ is a multiple of the bit rate, a resampling operation must be performed. This is illustrated in Figure 3 (a). The resample factor is explained in the next paragraph.

Recent work on pilot-assisted equalization in aeronautical telemetry [2]–[13] is the motivation for the problem considered in this paper. Here, a continuous-time telemetry receiver translates a 10.3125 Mbit/s SOQPSK-TG signal from RF (L or C band) to a 70 MHz IF. The IF signal is sampled in prepration for the application of discrete-time equalization techniques. The desire is produce I/Q samples at a sample rate equivalent to 2 samples/bit, or 20.625 Msamples/s.

The challenge with implementing the block diagram in Figure 3 (a) is the complex heterodyne operation following the ADC. First, the samples of the sinusoids must be produced (or stored and accessed) at the IF sample rate. Second, the multiplications required for the complex heterodyne operation must be performed at the IF sample rate.

For this design, quadrature downconversion and resampling are performed in two steps. The first step involves quadrature downconversion and downsampling by an integer factor D. This is because proper selection of D and the IF sample rate removes the requirement to perform the multiplications by the complex exponential at the high sample rate. The second step is devoted purely to resampling and is based on a polyphase filterbank approach. The end result is the system of Figure 3 (b).

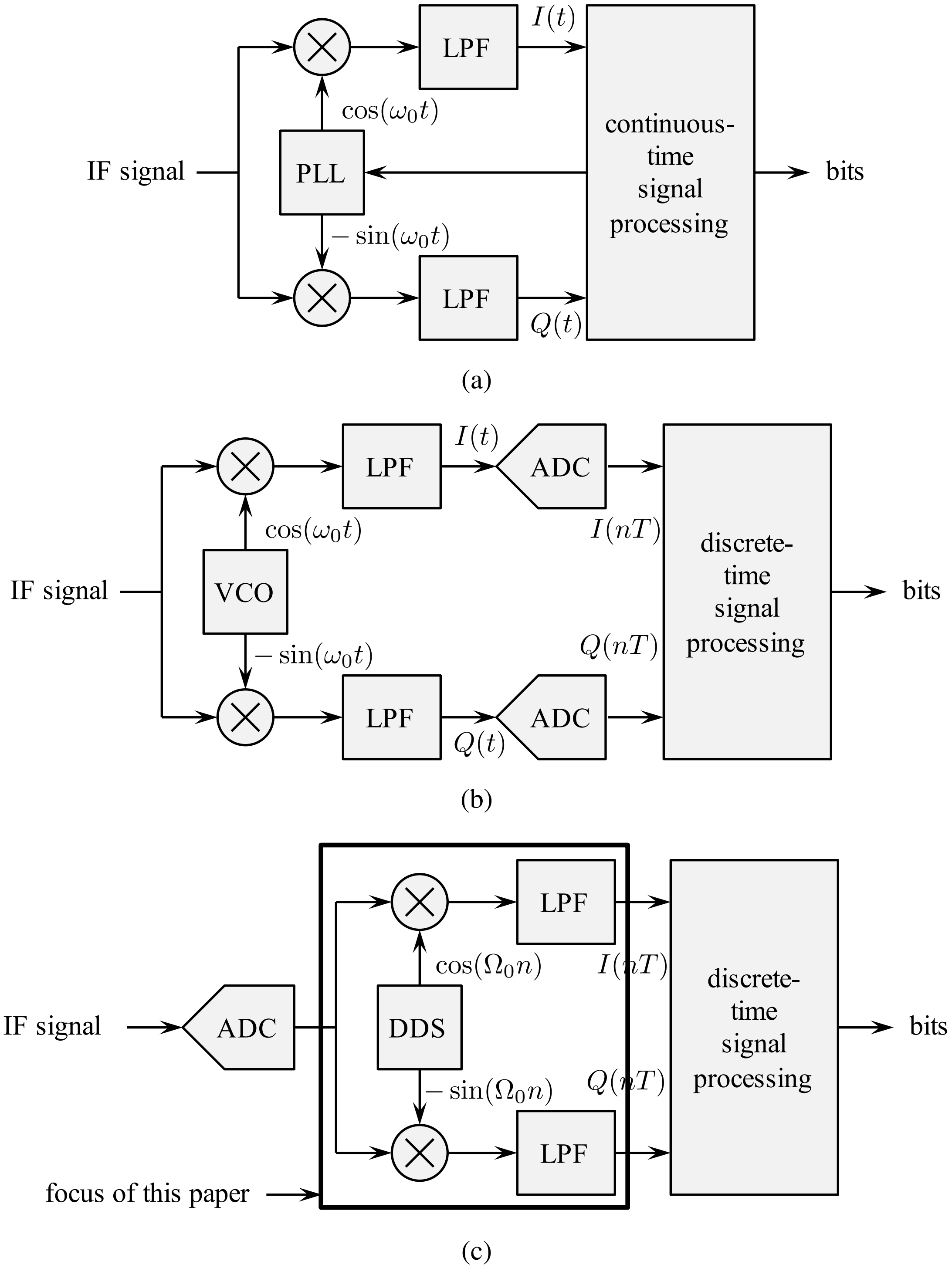

Figure 1: Generational evolution of receiver/demodulator architectures for digital communications: (a) first generation; (b) second generation; (c) third generation.

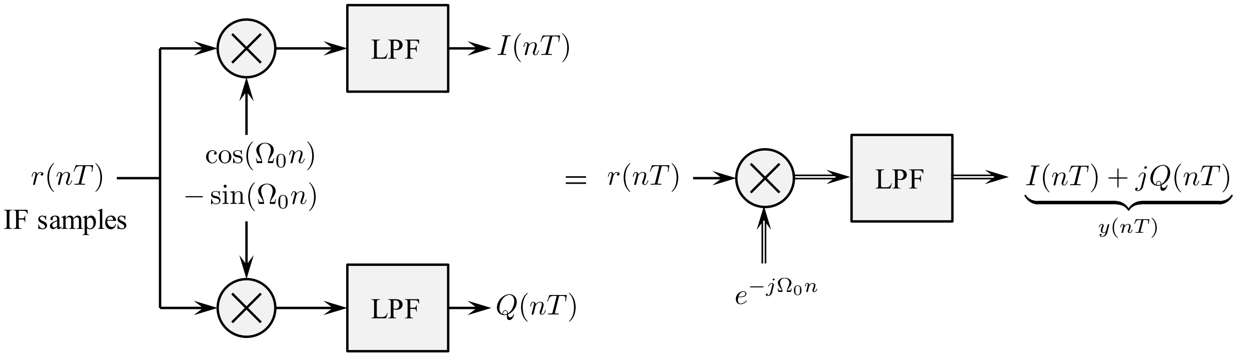

Figure 2: An illustration of the complex-valued equivalent processing based on Euler's formula (1).

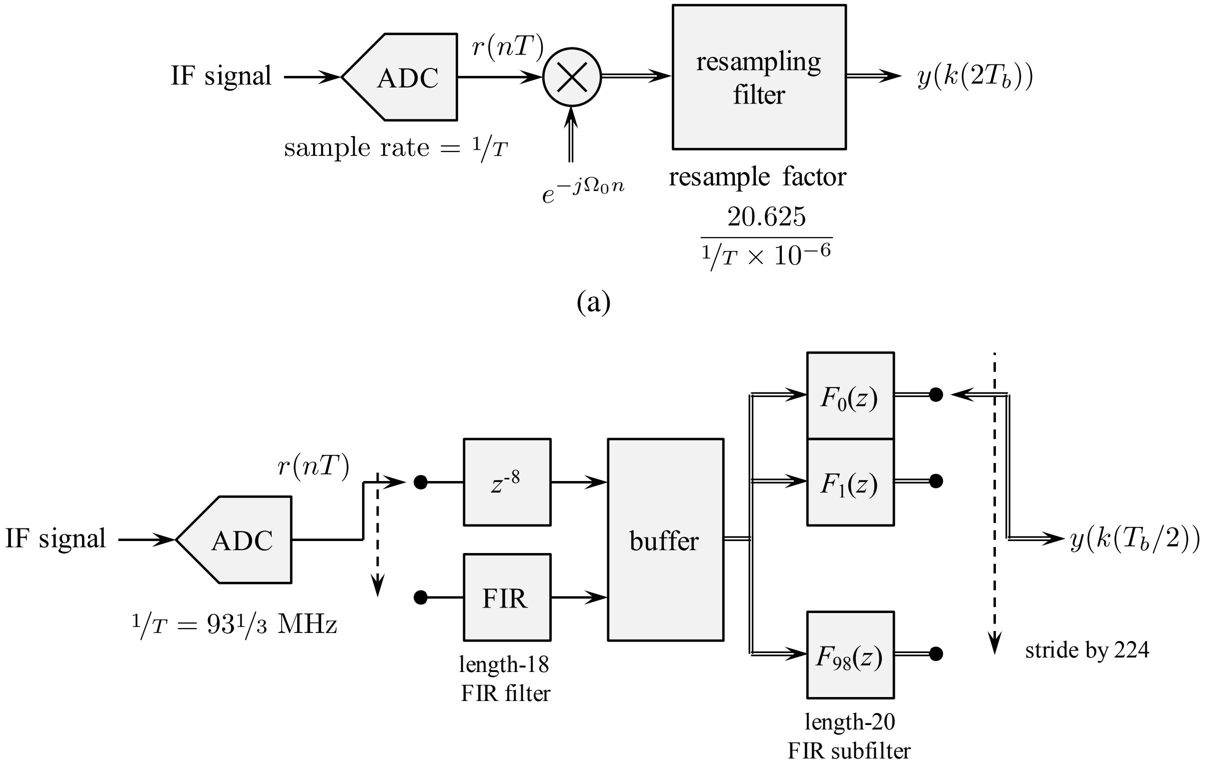

(a)

(b)

Figure 3: The required resampling operation: (a) the general problem formulation; (b) the solution using two polyphase filterbanks described in this paper.

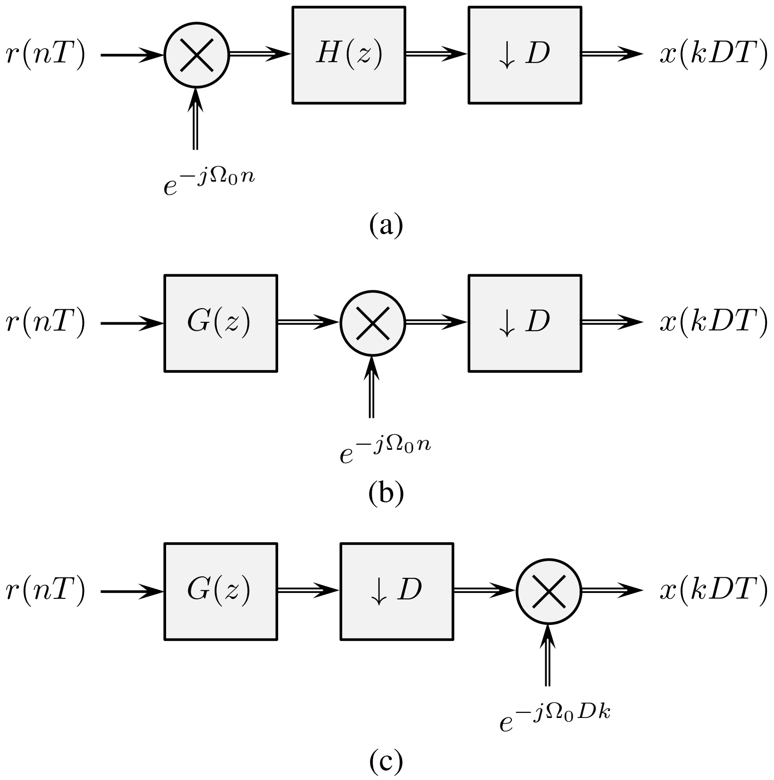

Figure 4: Three equivalent versions of downconvert/filter/downsample: (a) downconversion → low-pass filter → downsample; (b) bandpass filter → downconversion → downsample; (c) bandpass filter → downsample → downconversion.

FIRST STAGE DESIGN

Bandpass Processing in Sampled Data Systems. The first stage performs quadrature downconversion and downsampling by an integer factor D. The situation is illustrated in Figure 4 (a). The output of the low-pass filter is

$$x(nT) = \sum_{\ell=0}^{L-1} h(\ell)x(n-\ell)e^{-j\Omega_0(n-\ell)} \tag{2}$$

which may be re-expresssed as

$$= e^{-j\Omega_0 n}\sum_{\ell=0}^{L-1} \underbrace{h(\ell)e^{j\Omega_0\ell}}_{g(\ell)} x(n-\ell) = e^{-j\Omega_0 n}\sum_{\ell=0}^{L-1} g(\ell)x(n-\ell). \tag{3}$$

In Equation (3), the filter coefficients $g(n)$ are result of heterodyning the low-pass filter coefficients $h(n)$. Consequently, $g(n)$ is the impulse response of a band-pass filter centered at Ω_0 rads/sample. Equation (3) defines the system shown in Figure 4 (b).

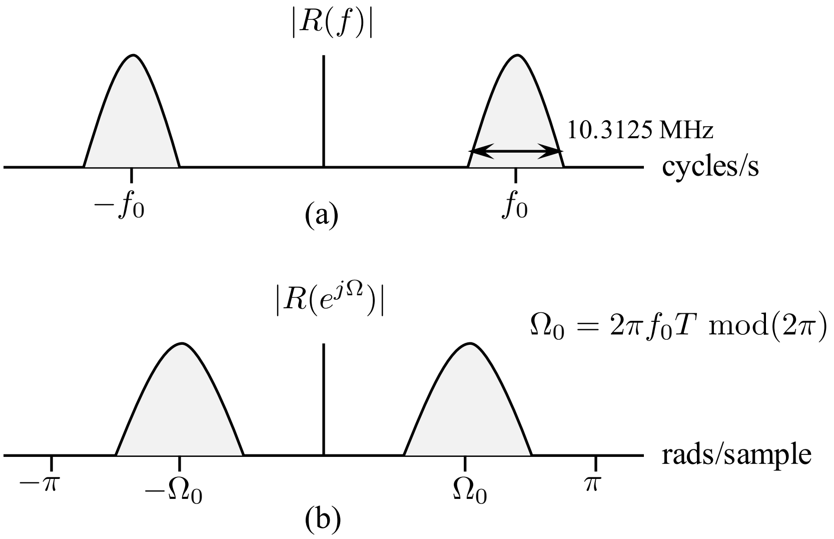

Figure 5: The relationship between spectrum of the continuous time IF signal (a) and the sampled IF signal (b).

The connection between the relationship (2) [illustrated in Figure 4 (a)] and the relationship (3) [illustrated in Figure 4 (b)] in the frequency domain is shown in Figures 5 and 6. The relationship (2) describes a frequency translation of the input signal spectrum to the left by Ω_0 rads/sample; this is illustrated by the black arrows in Figure 6 (a). This operation moves the desired spectrum (the positive-frequency component in this case) to baseband where it is isolated by the low-pass filter $H(z)$ as shown. In contrast, the relationship (3) creates a band-pass filter centered at Ω_0 rads/sample as shown in Figure 6 (b). The positive-frequency component of the input signal centered at Ω_0 is isolated at the band-pass filter output. The band-pass filter output is then translated to baseband as shown. The point is that both system are equivalent: they both produce the same result.

Polyphase Filterbank. Returning to Figure 4, Figure 4 (c) moves the downsample operation in front of the post-filter heterodyne. This move creates the familiar downsample-filter structure ideally suited to a polyphase filterbank. The polyphase decomposition of $G(z)$ may be derived by ordering the z-transform as follows. Let L be the length of $F(z)$. Assuming the downsample factor D divides the filter length L (i.e., $L = qD$ for some postive integer q), the z-transform may be expressed as

$$\begin{array}{rclclcccl} G(z) & = & g(0) & + & g(D)z^{-D} & + & \cdots & + & g((q-1)D)z^{-(q-1)D} \\ & + & g(1)z^{-1} & + & g(D+1)z^{-(D+1)} & + & \cdots & + & g((q-1)D+1)z^{-((q-1)D+1)} \\ & \vdots & & & & & & & \\ & + & g(D-1)z^{-(D-1)} & + & g(2D-1)z^{-(2D-1)} & + & \cdots & + & g(qD-1)z^{(qD-1)} \end{array} \tag{4}$$

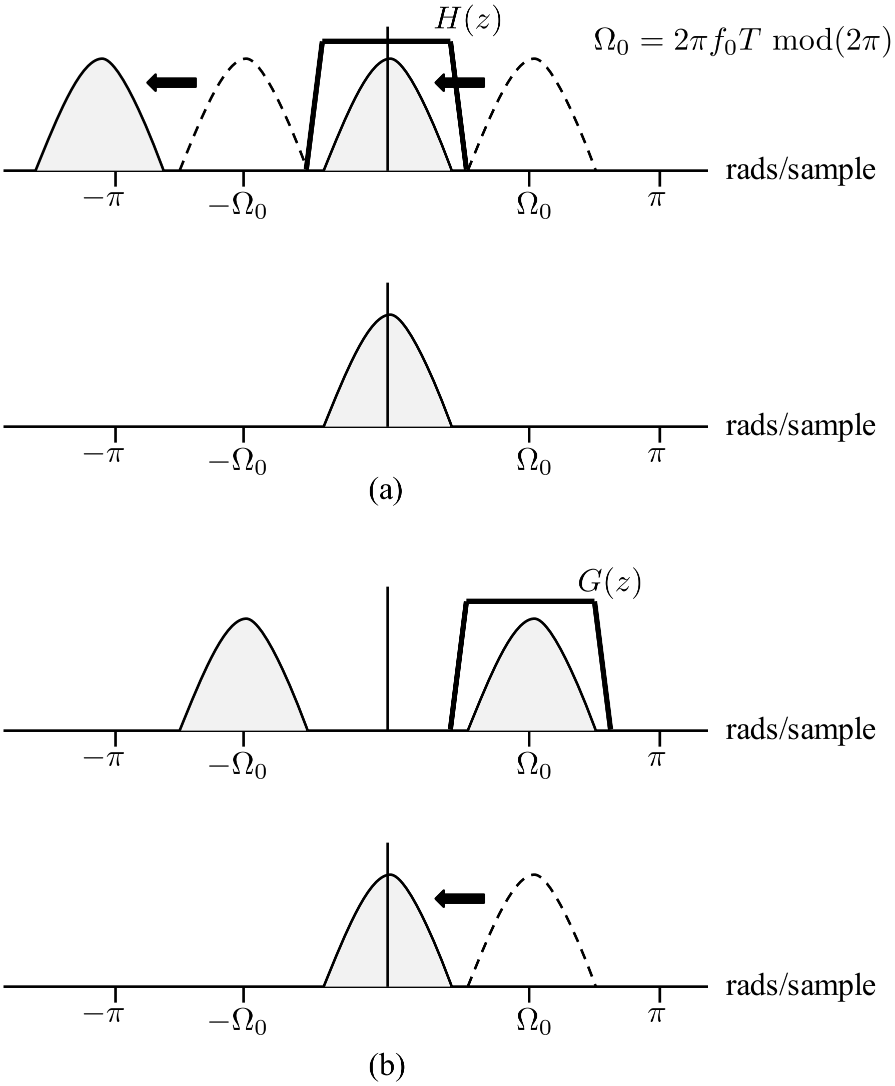

Figure 6: Frequency-domain interpretations: (a) frequency-domain interpretation of the relationship (2) [illustrated in Figure 4 (a)]; (b) frequency-domain interpretation of the relationship (3) [illustrated in Figure 4 (b)].

$$\begin{array}{rlllllll} G(z) & = & g(0) & + & g(D)z^{-D} & + & \cdots & + \;\; g((q-1)D)z^{-(q-1)D} \\ & + & z^{-1}\left[g(1)\right. & + & g(D+1)z^{-D} & + & \cdots & + \;\; \left.g((q-1)D+1)z^{-(q-1)D}\right] \\ & \vdots & & & & & & \\ & + & z^{(D-1)}\left[g(D-1)\right. & + & g(2D-1)z^{-D} & + & \cdots & + \;\; \left.g(qD-1)z^{(q-1)D}\right]. \end{array} \tag{5}$$

The polynomials inside the square brackets in each row define a z-transform in z^D. Consequently, the z-transform of $G(z)$ may be expressed as a sum of D z-transforms in z^D:

$$G(z) = G_0(z^D) + z^{-1}G_1(z^D) + \cdots z^{-(D-1)}G_{D-1}(z^D), \tag{6}$$

where

$$G_m(z^D) = g(m) + g(m+D)z^{-D} + g(m+2D)z^{-2D} + \cdots + g(m+(q-1)D)z^{-(q-1)D}. \tag{7}$$

The application of (6) to the system of Figure 4 (c) is illustrated in Figure 7 (a). Sliding the downsample operation from the filter output to the filter input produces the system shown in Figure 7 (b). Here the commutator operating on the input samples performs the downsample by D.

Using the substitution $g(\ell) = h(\ell)e^{j\Omega_0 \ell}$, $G_m(z)$ may be expressed as

$$\begin{aligned} G_m(z) &= h(m)e^{j\Omega_0 m} + h(m+D)e^{j\Omega_0(m+D)}z^{-1} + h(m+2D)e^{j\Omega_0(m+2D)}z^{-2} + \cdots \\ &\qquad + h(m+(q-1)D)e^{j\Omega_0(m+(q-1)D)}z^{-(q-1)} \\ &= e^{j\Omega_0 m}\Big[h(m) + h(m+D)e^{j\Omega_0 D}z^{-1} + h(m+2D)e^{j\Omega_0 2D}z^{-2} + \cdots \\ &\qquad + h(m+(q-1)D)e^{j\Omega_0(q-1)D)}z^{-(q-1)}\Big] \\ &= e^{j\Omega_0 m}H_m\left(e^{-j\Omega_0 D}z\right). \end{aligned} \tag{8}$$

Applying the relationship (8) to the system in Figure 7 produces the system shown in Figure 7 (c).

Equipped with the system in Figure 7 (c), we are now in a position to make design decisions to simplify the mathematical operations.

1. To eliminate the complex exponential operations at the filterbank inputs, the IF sample rate must be selected so that $\Omega_0 = 0, \pi/2$, or π. $\Omega_0 = 0$ is not possible because this requires colocating the positive and negative frequency components of the continuous-time IF spectrum in Figure 5 (a) at $\Omega_0 = 0$. This cancels the quadrature component of the IF signal. A similar problem occurs with $\Omega_0 = \pi$. The only workable solution is $\Omega_0 = \pi/2$. Here each input sample is "multiplied" 1, j, -1, or $-j$. "Multiplication" by 1 requires no resources, and "multiplication" by -1 is a simple sign switch. Similarly, multiplication by $\pm j$ simply assigns the real-valued input sample to the imaginary component of the filter input.

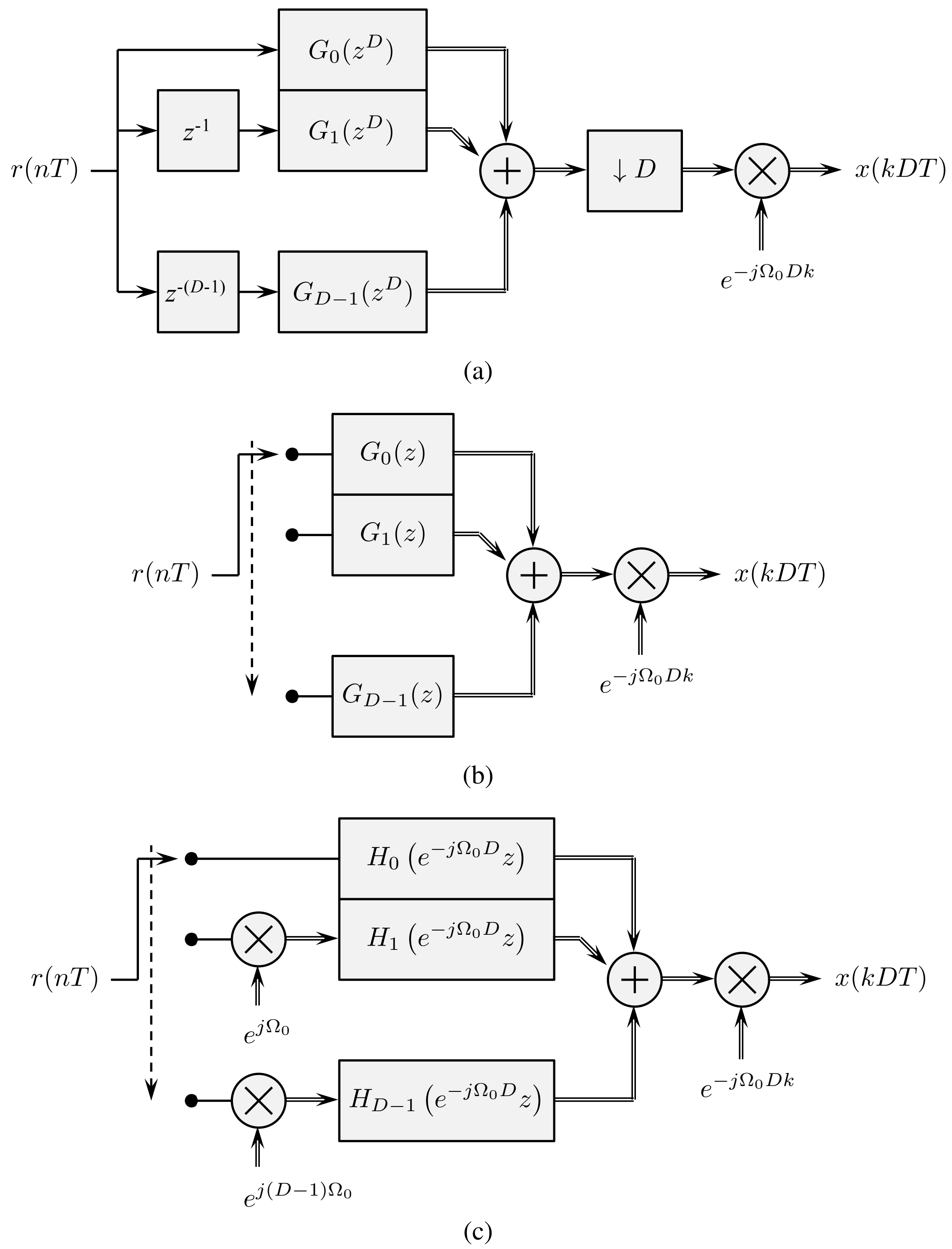

Figure 7: A polyphase decomposition of the system of Figure 4 (c): (a) the system of Figure 4 (c) with the polyphase decomposition of $G(z)$ used in place of $G(z)$; (b) the system of part (a) with downsample operation translated to the input; (c) the polyphase bandpass filter $G(z)$ replace by the equivalent version of the low-pass filter $H(z)$.

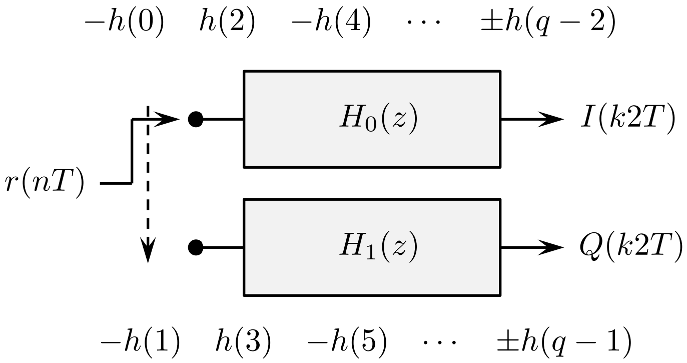
$-h(0)$ $h(2)$ $-h(4)$ $\cdots$ $\pm h(q-2)$
$H_0(z)$
$I(k2T)$
$r(nT)$
$H_1(z)$
$Q(k2T)$
$-h(1)$ $h(3)$ $-h(5)$ $\cdots$ $\pm h(q-1)$

Figure 8: The special case of the system in Figure 7 (c) for $\Omega_0 = {}^{\pi}\!/\!{}_{2}$ and $D = 2$.

2. The complexity of the polyphase filter bank can be reduced by a factor of 2 if all of the filter coefficients are real. Equation (8) shows that this occurs when when

$$\Omega_0 D = \pi \bmod(2\pi) \quad \text{or} \quad \Omega_0 D = 0 \bmod(2\pi). \tag{9}$$

In the first case, $g_m(n) = \pm h_m(n)$. In the second case, $g_m(n) = h_m(n)$. Using $\Omega_0 = \pi/2$, as argued previously,

$$\begin{aligned} \Omega_0 D &= \frac{\pi}{2} D = \pi \implies D = 2 \\ \Omega_0 D &= \frac{\pi}{2} D = 2\pi \implies D = 4. \end{aligned} \tag{10}$$

Because using $D = 2$ simplifies the resampling filter in the second stage, $D = 2$ is assumed in the remainder of this paper.

3. The post filter heterodyne operation involves the complex exponential

$$e^{-j\Omega_0 Dk} = e^{-j\pi k} = (-1)^k. \tag{11}$$

Thus, the final heterodyne operation reduces to sign alternations applied to the filter output. It is easy to show that the sign alternations may be moved to filter coefficients. (This sign alternation is in addition to the sign alternations in item 2.)

The special case of the system in Figure 7 (c) corresponding to $\Omega_0 = {}^{\pi}\!/\!{}_{2}$ and $D = 2$ is illustrated in Figure 8. The multiplier on the input to $H_1(z)$ reduces to $e^{j\Omega_0(D-1)} = e^{j\pi/2} = j$. This is not really a multiplication, but rather assigns all odd-indexed IF samples to the imaginary portion of the output. Because the imaginary portion is the quadrature component (see Figure 2), the lower branch produces the samples of the quadrature component at half the IF sample rate. The upper branch produces samples of the inphase component at half the IF sample rate.

With $\Omega_0 = {}^{\pi}\!/\!{}_{2}$ and $D = 2$, the remaining issues are IF sample rate and prototype filter design.

IF Sample Rate. The IF sample rate F_s that places the spectrum of the IF samples at $\Omega_0 = {}^{\pi}/_{2}$ rads/sample satisfies the relationship [1]

$$kF_s \pm \frac{1}{4}F_s = f_0 \tag{12}$$

where f_0 is the IF center frequency. Using $f_0 = 70$ MHz, the values of F_s produced by (12) that accommodate a bandwidth greater than 10 MHz are given in Table 1. For our problem, any of these would work [see Figure 5 (a)]. By far, the most common IF sample rate is the second entry $93{}^{1}/_{3}$ Msamples/s. Consequently, we use this value in our design.

Prototype Filter Design. Moving to the prototype filter design. The spectral requirements for this filter are summarized in Figure 9. Because the downsample factor is $D = 2$, the ideal lowpass filter is one with a cut-off frequency of $\pi/2$. A practical filter requires a transition band and a specification for the minimum allowable stop-band attenuation. Here we chose 60 dB for the stop-band attenuation (a common value in sampled-data systems) and, because the IF signal is oversampled, we use $0.4\pi < \Omega < 0.6\pi$ as the transition band. The filter length is the shortest length that achieves the desired stop band attenuation. The result is the length $L = 35$ filter illustrated in Figure 10. The top plot shows the impulse response $h(n)$ for $-17 \leq n \leq 17$. The lower plot in Figure 10 plots the DTFT of the prototype filter. The filter easily meets the stop-band attenuation requirement.

Observe that the $h(n) = 0$ for n non-zero and even and that $h(0) = 1$. This is characteristic of *half-band filters* [1]. Consequently, the top subfilter of Figure 8 is simply $H_0(z) = z^{-8}$. The subfilter $H_1(z)$ is

$$H_1(z) = h(-17) - h(-15)z^{-1} + h(-13)z^{-2} - \cdots - h(17)z^{-17}. \tag{13}$$

Note the sign reversals here. The sign reversals are required to compensate for the fact that using $F_s = 93\,{}^{1}/_{3}$ Msamples/s with $f_0 = 70$ MHz produces a spectral reversal.[1]

The polyphase filterbank of Figure 8 forms the first stage of the final solution shown in Figure 3 (b).

SECOND STAGE DESIGN

The output of the first stage produces a complex-valued sample sequence, where the real part corresponds to the inphase component of the IF signal and the imaginary part corresponds to the quadrature component of the IF signal, all sampled at half the IF sample rate (the sample rate here is

[1] Spectrum reversal here occurs because the negative-frequency component of the continous-time signal aliases to the positive frequency component of the sampled sequence. Consequently, the negative frequency component of the sample sequence is the desired sequence. This is change can be made by changing the sign on the complex exponential mixer input in Figure 4 (a) and tracking this change through the subsequent development.

Table 1: A partial list of IF sample rates that alias the IF spectrum to the quarter sample rate.

F_s (Msamples/s)	Usable Bandwidth (MHz)	Spectrum Swap
280	140	No
$93\,^1\!/_3$	$46\,^2\!/_3$	Yes
56	28	No
40	20	Yes
$31\,^1\!/_9$	$15\,^5\!/_9$	No
$25\,^5\!/_{11}$	$12\,^8\!/_{11}$	Yes
$21\,^7\!/_{13}$	$10\,^{10}\!/_{13}$	No

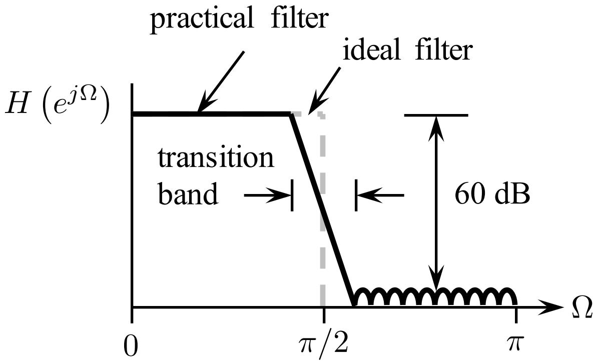

Figure 9: Spectral requirements for the prototype low-pass filter $H(z)$.

$46\,^2\!/_3$ Msamples/s). The desired sample rate is 2 samples/bit or 20.625 Msamples/s. Consequently the requirement for the second stage is to resample the output of the first stage by the factor

$$R = \frac{20.625}{46\,^2\!/_3} = \frac{99}{224}. \tag{14}$$

The brute force method for accomplishing this is to upsample the first stage output by 99 then downsample the result by 224. The upsample operation uses the familiar "upsample → filter" structure and the downsample operation uses the familiar "filter → downsample" structure. The approach is illustrated in Figure 11, where the (ideal) filter requirements are also shown.

The brute force approach of Figure 11 may be simplified in two steps.

1. The first step is to recognize that the cascade of a low-pass filter with cut-off frequency $^\pi\!/_{99}$ rads/sample with another low-pass filter with cut-off frequency $^\pi\!/_{224}$ rads/sample is simply a low-pass filter with cut-off frequency $^\pi\!/_{224}$. This is shown in the top portion of Figure 12.

2. Even with the replacement of the cascade of the two low-pass filters by a single low-pass filter, the system shown in the top portion of Figure 12 is still not practical. This is because the

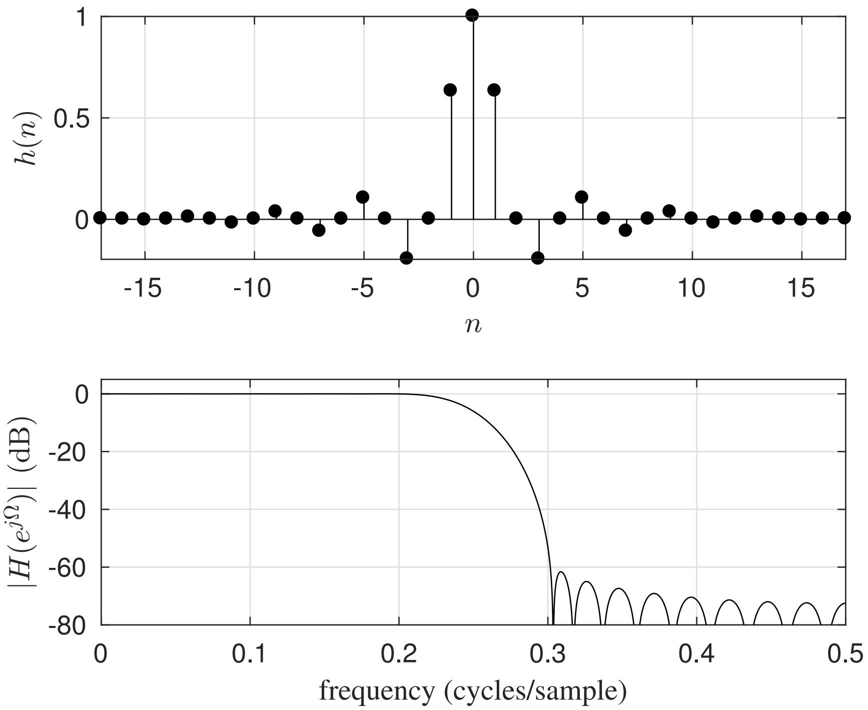

Figure 10: The prototype lowpass filter design.

filter must operate at the intermediate sample rate 99 times the input sample rate! Assuming the length of $F(z)$ is a multiple of 99, a polyphase decomposition may be used to perform the upsample operation. This is shown in the lower portion of Figure 12. The downsample operation simply strides through the polyphase filterbank outputs as shown.

Prototype Filter Design. The spectral requirements for the prototype filter $F(z)$ are summarized in Figure 13. The ideal filter has a cut-off frequency at $^{\pi}/_{224}$ rads/sample. The practical filter must have a transition band. Given the signal properties, a narrow transition band must be used. The filter was designed using $^{\pi}/_{224} < \Omega < {}^{2\pi}/_{224}$ rads/sample as the transition band. As before a stop

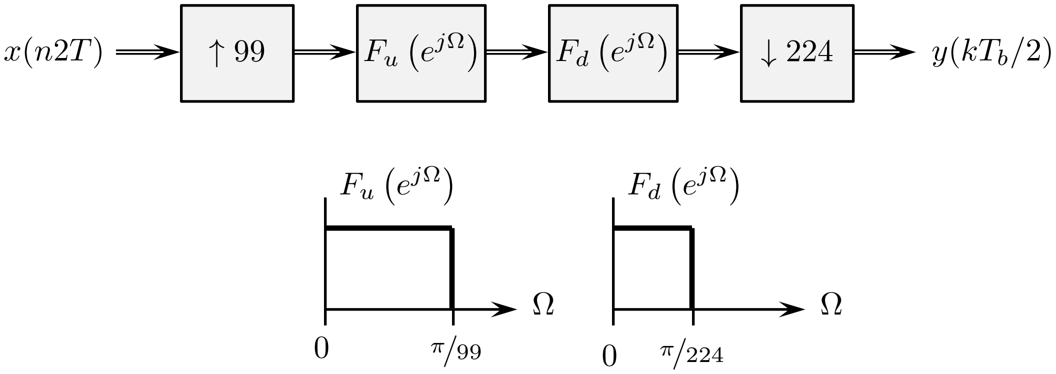
$x(n2T)$
$\uparrow 99$
$F_u\left(e^{j\Omega}\right)$
$F_d\left(e^{j\Omega}\right)$
$\downarrow 224$
$y(kT_b/2)$
$F_u\left(e^{j\Omega}\right)$
Ω
0
$^{\pi}/_{99}$
$F_d\left(e^{j\Omega}\right)$
Ω
0
$^{\pi}/_{224}$

Figure 11: A brute force approach to resampling by $^{99}/_{224}$.

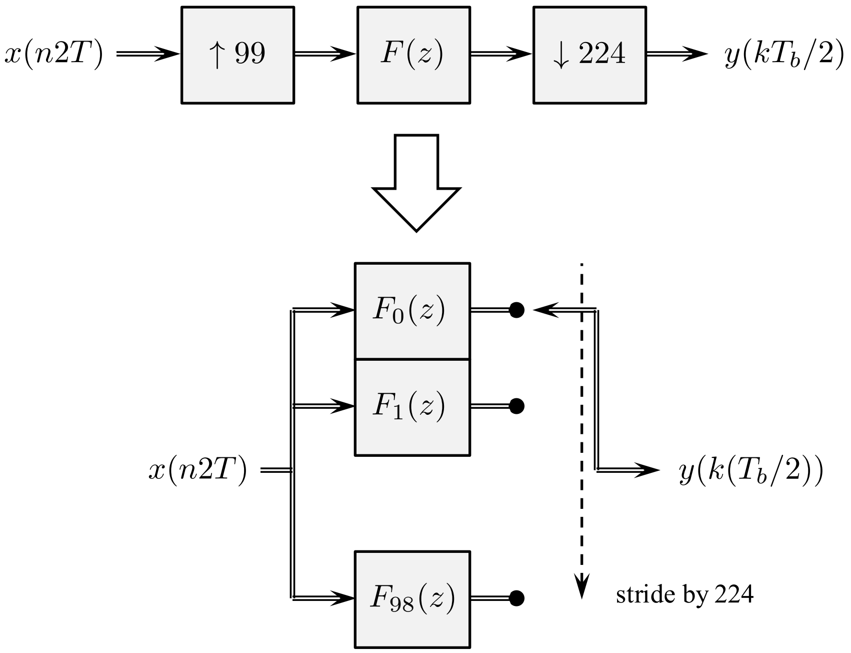

Figure 12: A block diagram of the resampling operation: (top) a conceptual block diagram; (bottom) the polyphase filterbank implementation.

band attenuation of 60 dB is also required. The filter length—defined as the smallest multiple of 99 that meets the stop-band attenuation requirements—is $20 \times 99 = 1{,}980$. The filter and its DTFT are shown in Figure 14.

Operation. The system shown in the lower portion of Figure 12 operates at half the IF sample rate on the input and at 2 times the bit rate on the output. Conceptually, each input sample produces 99 possible outputs, of which only 1 in 224 is required. The first few occurrences in the pattern are illustrated listed in Table 2. The pattern alternates between computing one output for every two inputs and computing one output for every three inputs in a structured way. The table ends with the 224-th input sample that produces the 99-th output sample (i.e., the resampling by $^{99}/_{224}$ means 99 output samples are produced for every 224 input samples). The pattern of subfilter indexes repeats at this point.

In general, the k-th output $y(k)$ is computed from the m-th subfilter using samples $x(n), x(n-1), \ldots, x(n-19)$:

$$y(k) = \sum_{\ell=0}^{19} f_m(\ell) x(n-\ell). \tag{15}$$

The block diagram in the lower portion of Figure 12 suggests that the digital hardware implementation comprises 99 length-20 FIR filters. But because the data in each filter is the same, the reality is that only a single length-20 FIR be implemented in hardware. When the proper samples have been clocked into the filter register, the coefficients corresponding to the desired subfilter are used to compute the output.

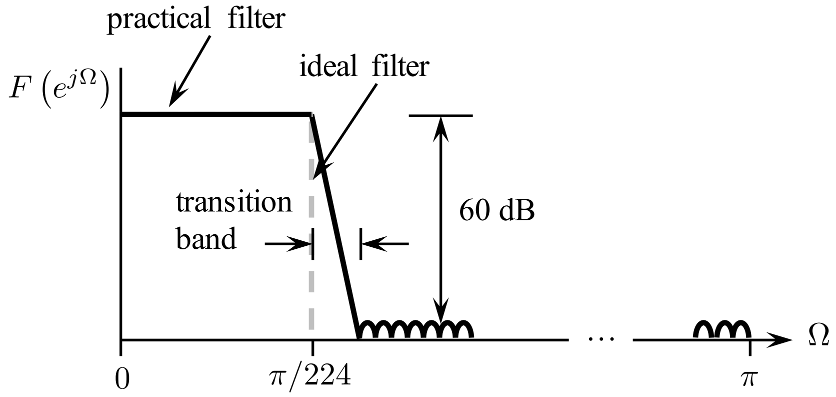

Figure 13: Spectral requirements for the prototype low-pass filter $F(z)$.

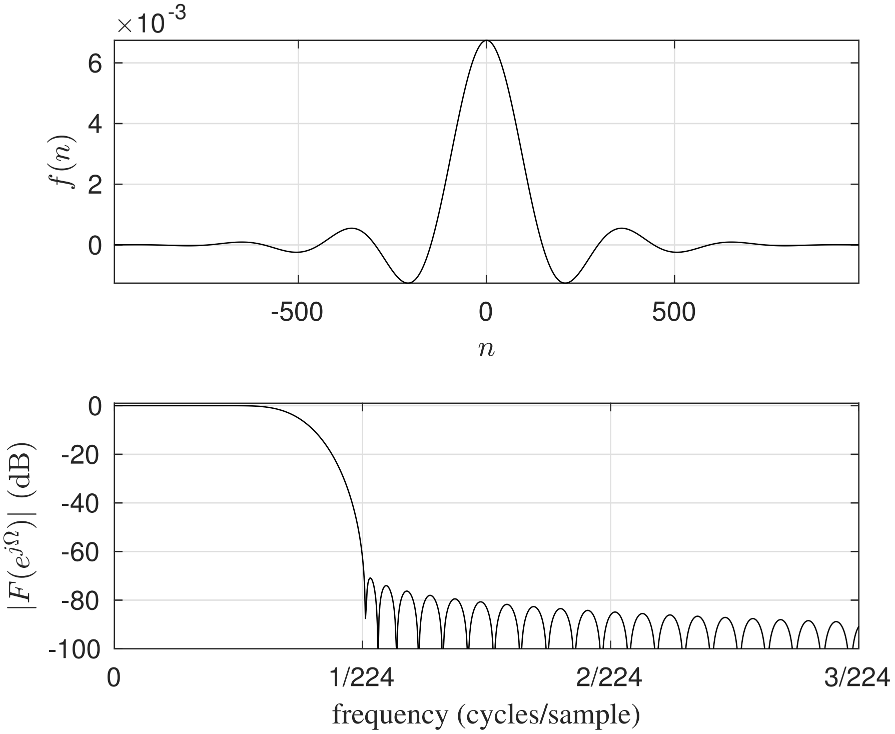

Figure 14: The prototype lowpass filter design for the resampling filter.

The convolution (15) may also be interpreted as an inner product:

$$y(k) = \begin{bmatrix} f_m(0) & \cdots & f_m(19) \end{bmatrix} \begin{bmatrix} x(n) \\ \vdots \\ x(n-19) \end{bmatrix}. \tag{16}$$

Because many digital hardware platforms are equipped with high-performance built-in inner product engines, the interpretation (16) can be leveraged to advantage. As the index pointer slides through the first stage outputs $x(n)$, each desired output is computed by forming the inner product of the length-20 first stage outputs and the appropriate vector of filter coefficients.

Table 2: The relationship between the input sample index, the polyphase filterbank index, and the output sample index.

input sample index	polyphase filter	output sample index
0	F_0	0
1	–	–
2	F_{26}	1
3	–	–
4	F_{52}	2
5	–	–
6	F_{78}	3
7	–	–
8	–	–
9	F_5	4
10	–	–
11	F_{31}	5
⋮		
221	F_{73}	98
222	–	–
223	–	–
224	F_0	99

CONCLUSIONS

This paper summarized the design of a discrete-time quadrature downconversion and resampling processor that operates on samples of 70 MHz IF signal. The unique properties of discrete-time processing—aliasing due to resampling bandpass signals and polyphase filter decompositions—were applied to create a low-complexity approach that does not require any arithmetic operations at the IF sample rate. The required tasks were performed in two stages. The basic principles were highlighted along the way to provide a roadmap for designs that meet different requirements.

ACKNOWLEDGEMENTS

This project is funded by the Test Resource Management Center (TRMC) Test and Evaluation, Science & Technology (T&E/S&T) Program through the U.S. Army Program Executive Office for Simulation, Training, and Instrumentation (PEO STRI) under Contract No. W900KK-13-C-0026

(PAQ). The Executing Agent and Program Manager work out of the AFTC.

REFERENCES

[1] M. Rice, *Digital Communications: A Discrete-Time Approach.* Upper Saddle River, NJ: Pearson Prentice-Hall, 2009.

[2] M. Rice, A. McMurdie, and E. Perrins, “A low-complexity preamble detector for iNET-formatted SOQPSK,” in *Proceedings of the IEEE Military Communications Conference*, (Baltimore, MD), pp. 718–723, 6–8 October 2014.

[3] M. Rice and E. Perrins, “On frequency offset estimation using the iNET preamble in frequency selective fading channels,” in *Proceedings of the IEEE Military Communications Conference*, (Baltimore, MD), pp. 706–711, 6–8 October 2014.

[4] M. Rice, M. Saquib, M. S. Afran, A. Cole-Rhodes, and F. Moazzami, “On the performance of equalization techniques for aeronautical telemetry,” in *Proceedings of the IEEE Military Communications Conference*, (Baltimore, MD), pp. 456–461, 6–8 October 2014.

[5] A. Cole-Rhodes, H. Umuolo, F. Moazzami, and M. Rice, “A block processing approach to CMA equalization of SOQPSK for aeronautical telemetry,” in *Proceedings of the IEEE Military Communications Conference*, (Baltimore, MD), pp. 456–461, 6–8 October 2014.

[6] M. Rice, C. Hogstrom, C. Nash, J. Ravert, A. Cole-Rhodes, F. Moazzami, M. Saquib, M. S. Afran, E. Perrins, and K. Temple, “Some initial results for data-aided equalizer experiments at Edwards AFB,” in *Proceedings of the International Telemetering Conference*, (Glendale, AZ), 8–10 November 2016.

[7] C. Hogstrom, C. Nash, and M. Rice, “Locating and removing preamble sequence in aeronautical telemetry,” in *Proceedings of the International Telemetering Conference*, (Glendale, AZ), 8–10 November 2016.

[8] J. Ravert and M. Rice, “On frequency offset compensation for equalized SOQPSK,” in *Proceedings of the International Telemetering Conference*, (Glendale, AZ), 8–10 November 2016.

[9] M. Rice, M. S. Afran, and M. Saquib, “Performance limits on joint estimation of frequency offset, channel, and noise variance in aeronautical telemetry,” in *Proceedings of the International Telemetering Conference*, (Las Vegas, NV), 26–29 October 2015.

[10] M. Rice, M. Saquib, and M. S. Afran, “MMSE equalization for aeronautical telemetry channels,” in *Proceedings of the International Telemetering Conference*, (San Diego, CA), 20–23 October 2014.

[11] M. Rice, M. Saquib, M. S. Afran, A. Cole-Rhodes, and F. Moazzami, “A comparison of three equalization techniques for iNET-formatted SOQPSK-TG,” in *Proceedings of the International Telemetering Conference*, (San Diego, CA), 20–23 October 2014.

[12] M. Rice, M. Saquib, and E. Perrins, “Estimators for iNET-formatted SOQPSK,” in *Proceedings of the International Telemetering Conference*, (San Diego, CA), 20–23 October 2014.

[13] A. Cole-Rhodes, H. Umuolo, F. Moazzami, and M. Rice, “Real-time CMA equalization for SOQPSK for aeronautical telemetry,” in *Proceedings of the International Telemetering Conference*, (San Diego, CA), 20–23 October 2014.